

Biological and mechanical response of laser shock peening orthopaedic titanium alloy (Ti-6Al-7Nb)

Proc IMechE Part H:
J Engineering in Medicine
2022, Vol. 236(8) 1169–1187
© IMechE 2022



Article reuse guidelines:
sagepub.com/journals-permissions
DOI: 10.1177/09544119221105849
journals.sagepub.com/home/pih



Xiaojun Shen¹, Pratik Shukla² , Sunita Nayak³, Vasanth Gopal⁴, Prabhakaran Subramanian⁴, Amy Sarah Benjamin³ and Shivpuram Kalainathan⁵

Abstract

This paper focuses on the evaluation of mechanical and biological properties of laser shock peening (LSP) orthopaedic grade Ti-6Al-7Nb alloy. LSP surface treatment was conducted at laser energy of 3 to 7 J with overlaps of 33%–67%, and with a 3 mm laser spot size. Cell viability on laser shock peened surface was evaluated through in-vitro MTT assay, using osteoblast-like MG63 cells for the first-time. Residual stresses, microhardness, microstructure, sliding wear and wetting properties were investigated. Compressive residual stresses were found at various depths due to controlling the LSP parameters, compared to the as-received surface. The laser shock peened surfaces were hardened from 365HV_{0.05} to 405HV_{0.05}, while the as-received surface was 320HV_{0.05}. The average sub-grain size was refined from 14% to 36% after LSP. The wear resistance was also controllable by altering LSP parameters. The MTT results show that the cell viability on the laser shock peened surfaces was comparatively lower than that of the untreated surface after 24 h. However, after 72 h, the cell viability on modified surfaces were significantly improved. This work indicated that laser shock peened surfaces have a strong potential to decrease the pain from orthopaedic implant failures and promote the cytocompatibility between the bone and implant.

Keywords

Laser shock peening, sliding wear, simulated body fluid, Ti-6Al-7Nb, cell viability

Date received: 20 May 2021; accepted: 25 April 2022

Introduction

Long-term osseointegration of implants with bones have always been one of the most crucial aims for considering the recovery of patients after implantations.¹ Once an implant is inserted into the human body, it would initially react with host issue, involving a series of physiochemical changes, ranging from molecular level to the cellular level.² The reaction determines the healing speed and long-term performance of implants, affected by the surface physicochemical properties of biomedical materials such as surface topography, wettability, electric properties, the pore size of biomaterials and bioactive molecules. Therefore, surface modifications to improve the biocompatibility of biomaterials are considered to be crucial to enhance the integration of interface where cell/protein adheres.

Although, surgical implant biomaterials such as metals, ceramics, and polymers are improved by a variety of surface modification techniques, namely: etching; blasting;

shot peening/ultrasonic peening; and non-contact, laser-based modifications. In particular, to acquire a certain surface roughness and enhance osseointegration, Flamant et al.,³ applied hydrofluoric acid (HF) to a dental ZrO₂ to increase roughness. It was found that a concentration of

¹School of Electrical and Electronic Engineering, Nanyang Technological University, Singapore

²The Manufacturing Technology Centre (MTC), Coventry, UK

³Centre for Biomaterials, Cellular, and Molecular Theranostics, Vellore Institute of Technology, Vellore, Tamil Nadu, India

⁴Department of Metallurgy & Materials Engineering, Faculty of Engineering, University of Malta, Msida, Malta

⁵Department of Physics, School of Advanced Sciences, Vellore Institute of Technology, Vellore, Tamil Nadu, India

Corresponding author:

Pratik Shukla, The Manufacturing Technology Centre (MTC), Ansty Park, Coventry CV7 9JU, UK.

Email: pratik.shukla@the-mtc.org

40% HF acid gave a uniform surface morphology with the shortest etching time. Blasting techniques including sandblasting, alumina blasting and micro-abrasive blasting are also useful methods to increase surface roughness to promote biocompatibility. Günay-Bulutsuz et al.,⁴ investigated the cell response of sandblasting on ultrafine and coarse titanium surfaces. Ultrafine and blasted surfaces are more biocompatible for human gingival fibroblast cells. Moreover, Granato et al.,⁵ evaluated the effect of micro-abrasive blasting and alumina-blast/acid-etching on pure Ti surfaces. In comparison to the as-machined surface, both the surface treatments in terms of roughness lead to the improvement of osseointegration in pure Ti substrates.

Therefore, a variety of surface modification methodologies or surface fabrication techniques, especially, the ones that are laser-based, were employed to improve the osseointegration of implants. Compared to conventional chemical methods, laser-based surface modifications enabled a wide variety of structures at the nano and the micro-scale, and the process is fast, reproducible, controllable and contactless. It is reported that laser introduces surface features such as grooves, dimples, lines that are beneficial in strengthening the bonding of implants and human bones.⁶ Raimbault et al.,⁷ evaluated the cell behaviour on a femtosecond laser-fabricated titanium surface at nanoscale and microscale level. Cells showed more sensitivity to the nanoscale structures. This indicated a potential for titanium modification in orthopaedic or dental applications. Batal et al.,⁸ employed a nanosecond pulse laser for surface texturing on CoCrMo alloy and compared the cell viability of Saos-2 osteoblast like cells on an as-received and various laser textured surfaces. A laser textured surface presented a better performance in terms of cell viability. Moreover, a CO₂ laser was used to modify the surface of nylon 6,6 and the mesenchymal stem cell was employed for evaluation. The viable cell counting increased to 60,000 cells/ml due to CO₂ laser surface treatment. Although, by applying a 3-D printing technique, the Young's modulus of orthopaedic scaffolds can be maintained close to that of bones with interconnected porous network, which favours the osseointegration and relieving the stress shielding effect.⁹ It is also a new promising direction for achieving long-term osseointegration of implants.

Laser Shock Peening (LSP) is also a very useful method for surface modification¹⁰ as it is more advanced in terms of penetration depth and quality of the part being treated. It has been widely and originally used in aerospace and auto industry for improving the fatigue properties of various metallic materials for decades.¹¹ It is promising that LSP could also be employed in extending implant service life by not only improving mechanical properties, but also enhancing the biocompatibility. LSP has its own advantages in medical applications, compared to conventionally employed surface modification techniques such as sandblasting, shot peening, laser texturing and so on.

For example, in comparison to sandblasting, no contaminations will be left after LSP. In addition, the top-most benefit will be induction of deeper compressive stress which is not available with sand, grit or shot blasting techniques. LSP is also a cold working method and laser would not contact metal surfaces directly rather than exploding the absorptive layer generating plasma-driven shock-waves, which causes material deformations. With the same capability like shot peening, LSP could also introduce a stable compressive residual layer in the treated materials.¹² However, when it comes to the complex medical implants, components such as acetabular, trabecular and proximal tibial, the focussed laser beam is able to precisely process the corner of the complex components, where conventional shot peening cannot reach, providing a better process control and benefit the material strength exactly where it is needed. Besides that, due to the microstructural deformation caused by high plasma pressure during peening, surface morphologies were generated by applying laser energy and foot-print, overlap, which means LSP also could benefit orthopaedic or dental implant osseointegration due to introducing certain surface roughness that increasing the surface roughness is critical for improving the biocompatibility. The features of topographies after LSP, namely: grooves and dimples, contribute to the cells/proteins adhesion and proliferation on the implant surfaces. This in turn strengthens the mechanical interlock between the implant and the bones. More than that, the stable compressive residual stress layer which benefits fatigue will be formed after LSP that is what other laser treatments (such as laser texture) are not capable of delivering.

When it comes to the mechanical properties of the implants, among the identified failure mechanisms of the implant, fretting wear is destructive to implant materials and occurs between two contacting solid bodies when exposed to relatively small amplitude oscillatory motion under a certain load.¹³ Such movements would generate fretting fatigue, which may cause material surface damage, thereby, acting as crack initiation sites.¹⁴ Furthermore, micro-cracks will extend from the material surface into the depth direction under the fretting fatigue leading to the reduction of fatigue strength. In a total hip implants system, the fretting wear normally occurs at the junction of head-neck that normally consists of titanium stem and ceramics.¹⁵ The metallic debris was considered to be the domain reason for causing osteolysis, and polyethylene debris would even cause implant degradation. This further results in aseptic loosening. Therefore, improving the wear resistance of a prosthesis is one of the main purposes of a surface enhancing technique.

As reported in our previous works and others,¹⁰ LSP has presented its capability to not only improve the wear resistance, but also alter the surface wettability of Ti-6Al-7Nb alloy by applying surface pattern and surface microstructure refinement. Zhou et al.,¹⁶ investigated the effects of LSP on friction and wear properties of medical Ti-6Al-4V alloy in Hank's solution. The

Table 1. Showing the chemical composition of Ti-6Al-7Nb alloy (units in wt%).

Element	Nb	Al	Ta	Fe	O	C	N	H	Ti
wt%	6.5–7.5	5.5–6.6	< 0.5	< 0.25	< 0.2	< 0.08	< 0.05	< 0.009	Bal

results showed that LSP can reduce debris peeling of Ti-6Al-4V implants. Zhang et al.,¹⁷ demonstrated that LSP not only decreased the co-efficient of friction and improved the wear resistance of AZ31B alloy, but also strengthened tensile strength and fatigue performance as well as enhance the corrosion resistance of metallic parts. Luo et al.,¹⁸ examined the effects of multiple treatments on electrochemical corrosion properties of Mg-Al-Mn alloy, and observed obvious improvement in electrochemical corrosion.

In this paper, a medical-grade Ti-6Al-7Nb alloy was treated with a Q-switch, Nd: YAG nanosecond pulsed laser. X-ray Diffraction (XRD), Scanning Electron Microscope (SEM) and Transmission Electron Microscope (TEM) were employed to observe both the microstructures and dislocation activities before and after LSP surface treatment. Mechanical property, namely, wear in simulated body fluid was investigated for the first-time subject to laser peened metals. On account of this, laser energy and overlap on the micro-hardness, tribological behaviour and worn surfaces are investigated by means of Vickers microhardness indentation, SEM and 3-D surface profiler. For a surface modification technique, the first and foremost aspect is that it should not be any cytotoxic to any biomaterials. Based on this prerequisite, an in vitro biological evaluation was carried with determining the cell viability of laser shock peened surfaces by using MTT cell proliferation assay for 24 and 72 h. The cell morphology was characterised by fluorescence microscope. In this work, the evaluation of the cell viability on the laser shock peened surfaces was conducted for the first-time. No other previous publications, hitherto, has shown investigations in relation to any parameters of laser shock peening discussed herein at any depth. In addition, the work could directly offer a new surface processing technique for improving both mechanical and biological properties of implants, thereby, directly benefiting the end-users who will be suffering the pain caused by implant failures such as corrosion, wear, fractures and loosening.

Experimental design

Material characterisations

Ti-6Al-7Nb alloy and surface characterisations. A medical grade hot rolled Ti-6Al-7Nb alloy with standard ASTM F1295 was deployed for the work herein. The chemical composition of the material is listed in Table 1. The material was provided by Aircraftmaterials co., Ltd, Stokenchurch, UK. The as-rolled Ti-6Al-7Nb rod was annealed at 870 °C for 4 h for stress relaxation purposes. The

Table 2. Laser shock peening parameters employed for the surface treatment of Ti-6Al-7Nb.

Parameters	Value
Pulse energy (J)	3, 5, 7
Laser wavelength (nm)	1064
Spot diameter (mm)	3
Number of laser impacts	1
Overlapping rate (%)	33%, 50%, 67%
Pulse duration (ns)	20
Radiance density ¹⁹ (W.mm ² .Sr.μm)	0.46 @ 3 J 0.77 @ 5 J 1.09 @ 7 J

microstructure of Ti-6Al-7Nb was characterised by a SEM (Sigma 500VP, manufactured by Zeiss, Germany) and a TEM (FEI, Tecnai-G² 20, The Netherlands) operating at 200 kV. Prior to SEM, mechanical grinding was carried out on a 3 mm-thickness disc by SiC abrasive paper from 320 grit to 2500 grit, followed by polishing from 9 to 1 μm and 2 h vibration final polishing to mirror finishing surfaces. Koll's reagent was employed for etching and each samples was carried out for 15secs. The TEM sample were cut from the top surface of the disc along the cross-section by wire-cut electrical discharge machining (EDM). Then the cut pieces were glued on a glass plate by a transparent thermoplastic glue and grinded to 100 μm. By heating the temperature, the TEM sample was carefully removed off the glass plate. Finally, the sample was thinned by a low-angle ion mill system until the material become electron transparent.

Experimental methods

Laser shock peening parameters. The laser shock peening experiments were conducted by a Q-Switched Nd:YAG laser with 3, 5 and 7 J at spot overlapping of 33%, 50%, and 67%. The detailed LSP processing parameters are given in Table 2. The water layer was used as the confinement layer (about 2 mm thickness), while the absorptive layer was a polyvinyl black tape. Figure 1(a) presents a schematic diagram of LSP, (b) experimental and theoretical laser shock peened samples and the schematic of LSP strategy.

Microhardness. Vickers hardness tester manufactured by Struer, Germany conducted the microhardness measurements. Each indentation was carried out with a load of 0.05 g along the longitudinal section of the laser shock peened specimen. The average value of each point was calculated three times in the same special area within the depth.

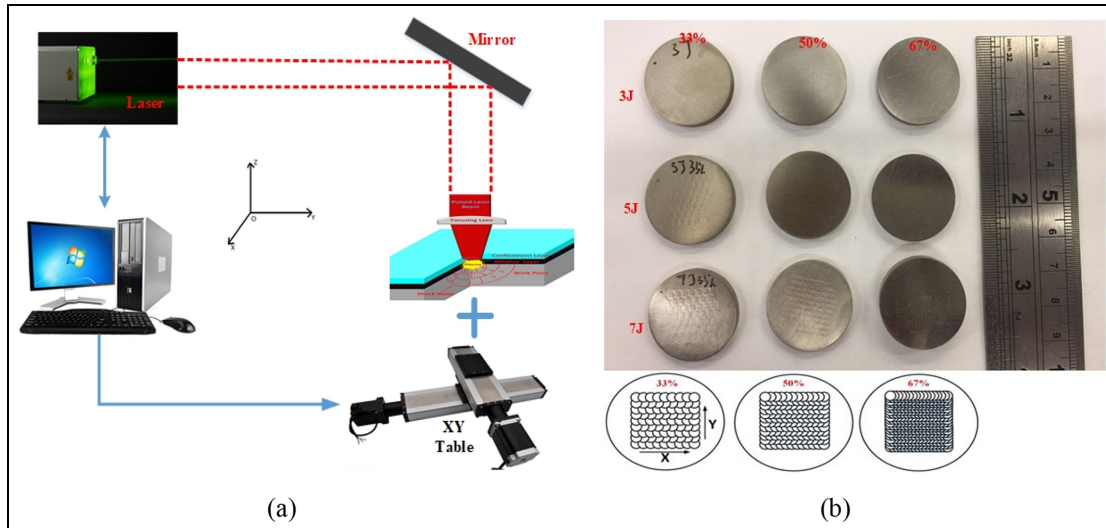


Figure 1. A schematic diagram of laser shock peening process in (a) and the schematics of the laser peening strategy in (b).

Wear testing. A ball-on-flat tribometer (manufactured by Ducom, India) with 6 mm diameter bearing grade ZrO_2 ball, was employed to conduct the reciprocating wear experiments. The Ti-6Al-7Nb samples prior to and after LSP were used as a flat material. Before the test, both counter moving ball and Ti-6Al-7Nb alloy were ultrasonically cleaned with isopropanol and distilled water. The wear test was conducted with a load of 5 N running for 18,000 cycles at frequency of 5 Hz and, the amplitude of the movement was $100 \mu\text{m}$. The displacement was fixed at $\pm 100 \mu\text{m}$, which is the minimum displacement that can be set with the tribometer. Faouvy energy ratio was not measured because the tribometer used in the current study does not plot fretting loop (frictional force vs displacement). The samples were placed in the specimen rig, immersed in 20% foetal bovine serum (FBS) solution (PH = 7.4), at the temperature of 37°C . The wear volume (V) of Ti-6Al-7Nb samples before and after LSP were calculated using Klaffke's equation (1)²⁰:

$$V(\text{mm}^3) = \pi R_h^2 \left(1 - \frac{h}{4R}\right)^4 \quad (1)$$

Where R is the radius of the counterpart; h is the depth of wear scar, π is pie (3.14) and 4 is a constant.

Wetting properties and residual stress. The residual stress measurements were carried out by using an incremental hole drilling method with a system designed by Stress Measurement, Shephed, UK. The measurement was conducted according to measurement good practice guide no.3²¹ and ASTM E837 standard.²² Regarding the dynamic contact angle measurement, a needle-in method was employed *via* an instrument OSCA1000 developed by Data physics co., Ltd, Germany. The measurement of dynamic contact angles was carried

out automatically with filming the course from wetting (advance contact angle) and de-wetting (receding contact angle). At the beginning, the volume of the drop was continuously increased to $10 \mu\text{l}$ with motorised piston. After keeping the syringe needle steady for 10 s, the volume of liquid was withdrawn off the solid surfaces at the same the images are recorded and evaluated.

Cell viability and fluoresce image. In order to check the biocompatibility against live cells the following assay was carried out. The metal samples were sterilised by washing with sterile water, ethanol and PBS and immersed in Dulbecco's Modified Eagle Medium (DMEM) w/o L-Glutamine incomplete media (HiMedia Laboratories, India) for about 15 days. The spent media with immersed samples and leachate if any, was used to carry out the study. Biocompatibility of the metal samples was evaluated using osteosarcoma cells (MG-63). The cells were grown in DMEM supplemented with 10% FBS, penicillin (100 I.U/ml) and streptomycin (0.1 mg/ml) all obtained from HiMedia Laboratories, India. The cells were maintained in a humidified incubator (ESCO Cellmate Biotech, Singapore) at 37°C with 5% CO_2 environment. The cells (MG-63) were seeded onto the 24 well plate at 1×10^4 cells per well and allowed to attach overnight with complete media. After 24 h the complete media was aspirated and replaced by the immersed media of the metal samples and the study was done for 24 and 72 h after the change.

After the first day and third day the (3-(4,5-Dimethylthiazol-2-yl)-2,5-Diphenyltetrazolium Bromide) MTT reagent (HiMedia Laboratories, India) was added (1 mg/ml) and incubated for 1 h. Thereafter, DMSO (Himedia) was added to dissolve the formed formazan crystals. The dissolved solution was transferred to 96 well plate and the absorbance was measured using a spectrophotometer (Read Well, Touch Robonik, India) at a

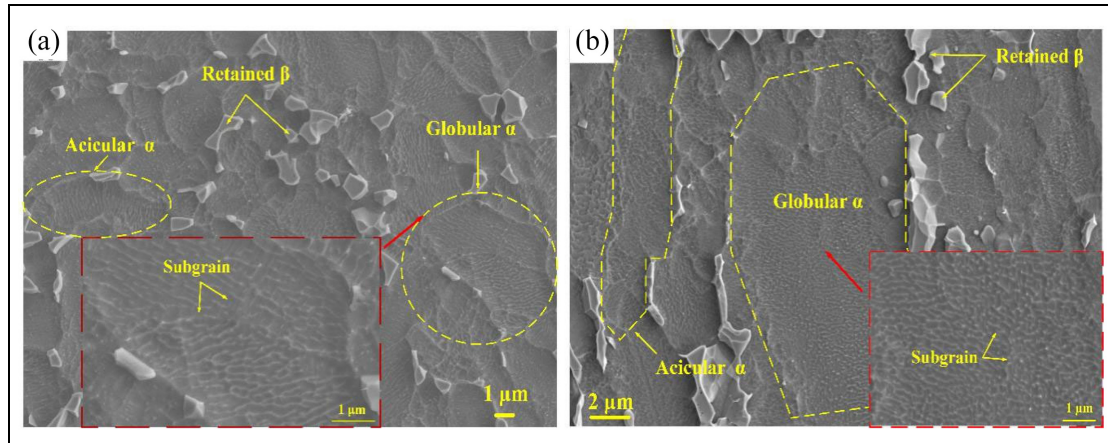


Figure 2. SEM images showing surface in (a) and longitudinal section in (b) of the microstructure of Ti-6Al-7Nb.

wavelength of 570 nm. Reported values are the mean of 3 replicates and expressed as percentages of the control values.

For fluorescence study, the metal samples were sterilised with ethanol followed by wash with PBS and kept in UV light overnight. Equal number of osteosarcoma cells (MG-63) (1×10^4 cells) were seeded on the surface of the metal samples. The cells were grown in DMEM supplemented with 10% FBS, penicillin (100 I.U/ml) and streptomycin (0.1 mg/ml). The cells were maintained in a humidified incubator (ESCO Cellmate Biotech, Singapore) at 37°C with 5% CO₂ environment. Very minimal amount of media was added initially to prevent the runaway of cells directly on to the surface treated well plate. After 4 h more media was added to the cells and allowed to culture. The imaging was done on the third day after 20 min of incubation of cells with nuclear staining dye 4',6-diamidino-2-phenylindole (DAPI from Himedia).

Statistical analysis. The whole experiment was repeated three times as mean values with standard deviation. The data were statistically analysed using analysis of variance (ANOVA) for assessing the significance level of the differences between the groups. The possibility p less than 0.05 was considered significant differences.

Results

Microstructure characterisation

As-received surface and cross-sectional microstructural characterisations. Both the as-received surface and the laser shock peened Ti-6Al-7Nb were characterised to find that laser shock peening affected grains, leading to grain refinement. This has a significant relationship with the mechanical properties of metal alloys.²³ The SEM images (as shown in Figure 2(a)) showed that the surface microstructure of as-received Ti-6Al-7Nb alloy consists of globular and acicular α and retained β grains. The acicular and globular α -grains distribute

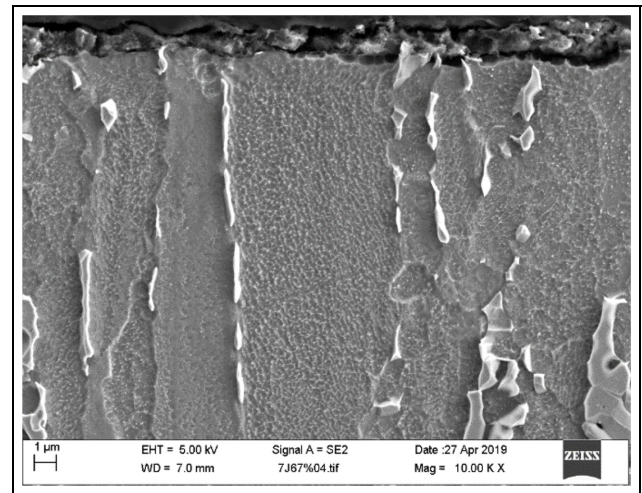


Figure 3. SEM images showing the longitudinal microstructure of Ti-6Al-7Nb subject to LSP parameter of 7J at 67%.

non-uniformly. The smaller α -grain surround around the large coarse one, and between them, retained β -grains, that were distributed randomly. What is more, the size of α -grain varies from several micrometres to tens of micrometres due to the hot rolling process. Observing at high magnifications, sub-grains are inside the coarse grains and the sub-grain boundaries are quite sharp. Cross-sectional microstructure is given in Figure 2(b), as mentioned above (hot rolling), the grains are elongated along rolling direction. Like surface, the grains also distribute randomly and non-uniformly. At higher magnification, we also can see sub-grains and sub-grains boundaries. With the grain intercept method (GIM), the as-received sub-grain size is 266.5 nm.

The longitudinal section microstructure of laser shock peened Ti-6Al-7Nb. Figure 3 shows the longitudinal section microstructure of Ti-6Al-7Nb alloy subject to LSP parameter of 7J, 67% (at the magnification of 10 K).

Table 3. The average sub-grain size (nm) after laser shock peening calculated by grain intercept method.

	33%	50%	67%
3J	251.08	216.9	185
5J	175.75	159.77	152.83
7J	152.83	146.46	140.4

Compared to the as-received microstructure, amongst all LSP parameters, there is no obvious sign showing that any refinement occurred by the grain size.

Therefore, increasing the magnifications to 40 K, inside coarse grains, the sub-grains were clearly observed as shown in Figure 4. With GIM, the average sub-grain size is presented in Table 3.

Phase determination by X-ray diffraction. The LSP induced high pressure shock waves could result in plastic deformation, the formation of residual stress and new microstructural phases in K403 nickel alloy.²⁴ In order to investigate the effects of LSP on the microstructure of Ti-6Al-7Nb, X-ray diffraction (XRD) method was conducted to measure the different diffraction patterns. Therefore, the XRD patterns of laser shock peened samples (2θ from 10° to 90°) are showed in Figure 5. It can be seen that the main phase of Ti-6Al-7Nb alloy are still peaks of $\alpha(100)$, $\alpha(002)$, $\alpha(101)$, $\alpha(102)$, $\alpha(110)$, $\alpha(103)$, $\alpha(200)$, $\alpha(201)$ and $\beta(110)$. There are not any new peaks formed after LSP. This indicates that there is no phase transformation and no new crystalline phases generated which is normally the case with laser shock peening of metals and alloys.

The peak broadening and shifting is shown in the magnified peaks images in Figure 5. This is due to the changes in lattice strain and crystallite size caused by high-strain plastic deformation. In the peak of $\alpha(100)$ (Figure 5(a-1), (b-1) and (c-1)), the peak was broadened with increasing the laser energy (if the overlap was kept constant). It is reported that if peaks shift towards higher 2θ angles, then the induced residual stress is compressive. However, we did not see such trend about the peak shifting relating the residual stress. Therefore, the broadening is the domain factor for examining the lattice strain and crystallite size.

TEM observation of dislocations at grain boundaries after laser shock peening. The microstructure in the region of top surface of laser shock peened Ti-6Al-7Nb alloy was characterised by using TEM shown in Figures 6 and 7. Published literatures has reported that LSP could lead to surface and near-surface microstructure deformation movements, especially high-density dislocations.^{25,26} At the top surface, there are many dislocations features including dislocation tangles, dislocation walls, dislocation cells, and dislocation pile-ups. In Figure 6(a) to (d), dislocation lines, dislocations walls are accumulated

near the grain interfaces as the impeding of the grain boundary. With increasing the density of dislocations, the dislocation tangles will transform into dislocation walls (Figure 6(e)). Furthermore, these will further form new sub-grain boundaries, and the sub-grains were even refined into nano-size which can be classified as 'Laser Shock Peening Nano-crystallisation' phenomenon.²⁷ It has been shown that the higher the density of the sub-grains, the higher the yield stress of material due to the increased sub-grain boundary. In Figure 6(f) and (g), more dislocations move towards the sub-grain or grain boundaries, and unable to pass the boundary, thereby, a process of 'pile-up' occurs at the grain boundary. The grain boundary strengthening theory has a great influence on the yield strength, as described by Hall-Petch relationship as shown in equation (2):

$$\sigma_y = \sigma_0 + \frac{k_y}{\sqrt{d}} \quad (2)$$

Where d is the grain size, σ_y is the yield stress, σ_0 is the material constant for the starting stress and k_y is the material strengthening co-efficient. This H-P relationship indicates that the smaller the grain size, the higher the applied stress needed to propagate dislocations through the material. Therefore, that is an important factor in the microstructural aspect that LSP can benefit the fatigue resistance of the metallic materials.

Figure 7(a) to (c) with the selected area electron diffraction (SEAD) was taken from top surface to the inner substrates. It can be seen from Figure 7, the SEAD pattern in the image was ring-shaped which indicated that the original sub-grains have been refined and the orientation distributed randomly. In Figure 7(b), there are high intensity dislocations forming dislocations tangles and dislocations wall. However, the corresponding SEAD image presents the arc-shaped diffraction patterns which means the sub-grain refinement has not been completed yet. A similar trend can also be found in Figure 7(c) corresponding SEAD image. There is some matrix apparent in the SEAD.

Mechanical properties

Residual stress. The residual stress distributions along the surface and sub-surface before and after LSP are presented in Figure 8. In terms of the untreated curves, the residual stress at the near surface is tensile due to the hot rolling process which rendered to uneven cooling. Although, the such residual stress is self-phase-balanced, it still affects the performance of titanium alloy under external. For instance, force deformation, stability, fatigue, and other aspects may have adverse effects. Therefore, surface modification method is necessary to change the metallic surface condition. In comparison, after LSP, the residual stresses are transferred into compressive by LSP from the near surface to a

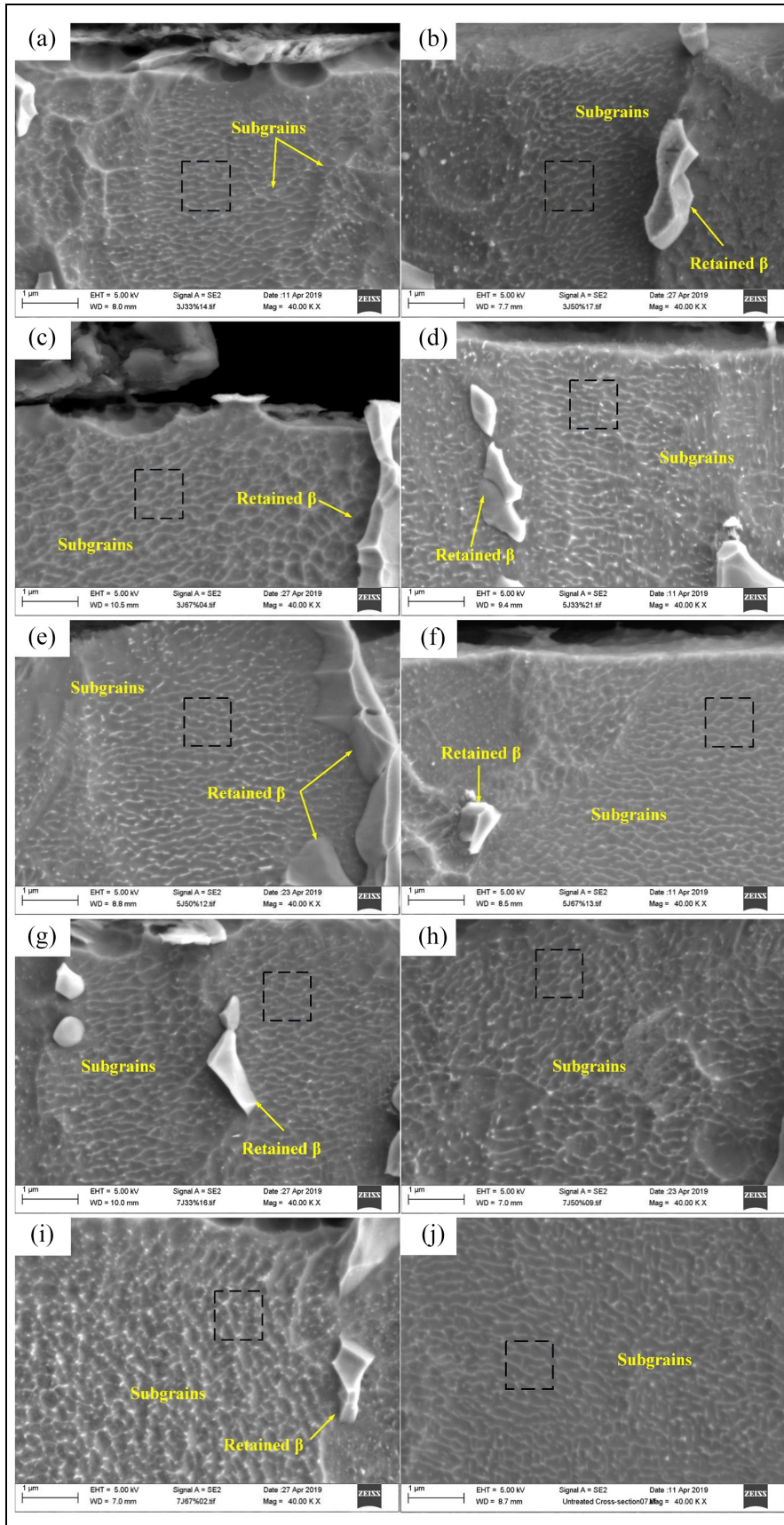


Figure 4. SEM images showing the sub-grains before and after laser shock peening at parameters of (a) 3 J, 33%, (b) 3 J, 50%, (c) 3 J, 67%, (d) 5 J, 33%, (e) 5 J, 50%, (f) 5 J, 67%, (g) 7 J, 33%, (h) 7 J, 50%, (i) 7 J, 67%, and (j) untreated.

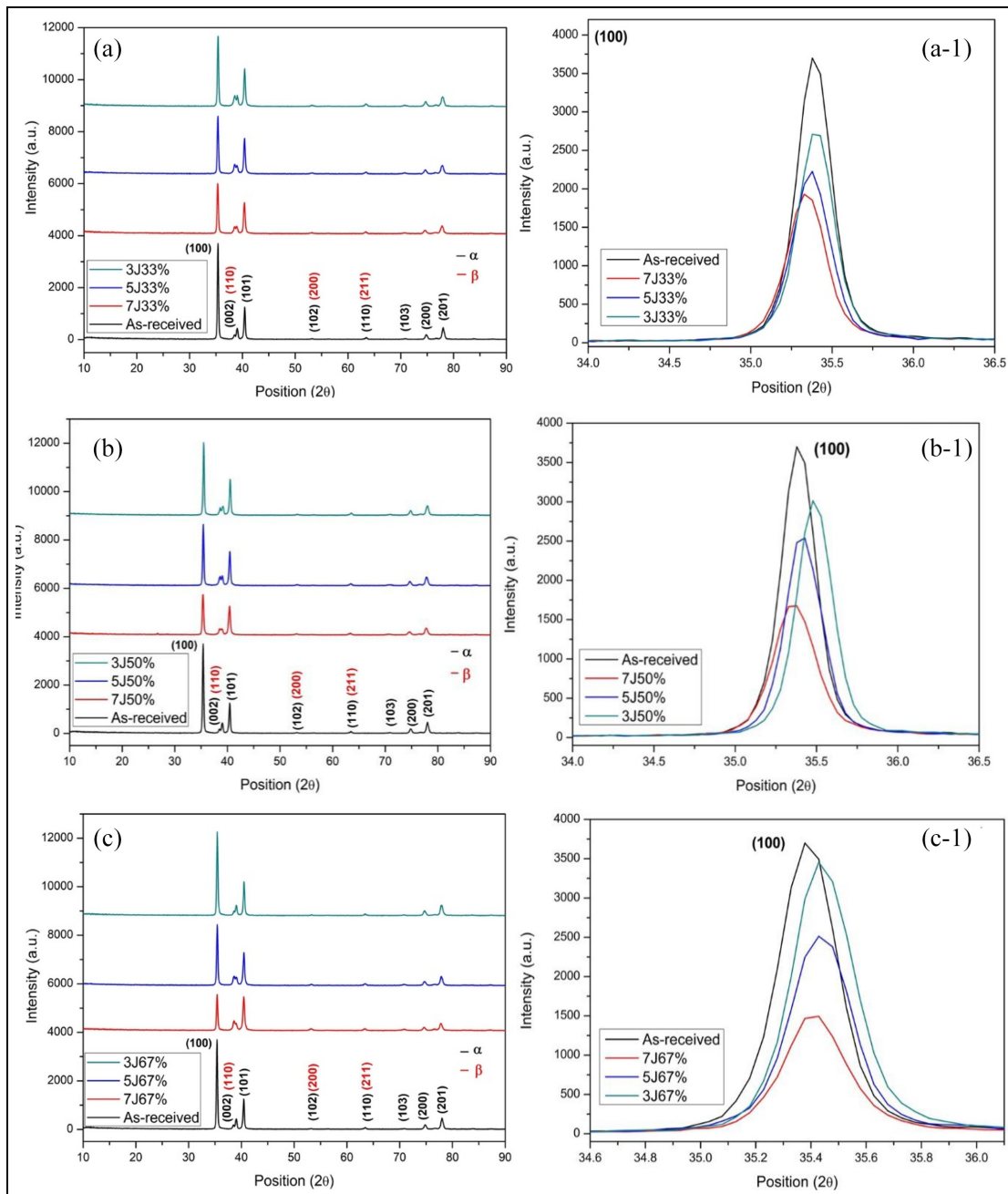


Figure 5. X-ray diffraction patterns and magnified α (100) peak of Ti-6Al-7Nb alloy in (a) 33%, (b) 50% and (c) 67%.

certain depth. More detailed info can be found in our previous published literature.²⁸

Surface hardness subject to laser shock peening. Improving micro-hardness can benefit the wear resistance, which is one of the main failure issues in many surface modification methods, as the main failure mode of orthopaedic implants is wear. The Vickers micro-hardness distributions in the cross-section of the Ti-6Al-7Nb alloy, before and after LSP are shown in Figure 9. The longitudinal section microhardness of the untreated scatters from 325HV_{0.05} to 335 HV_{0.05}. After laser

shock peening, it was seen that the Ti-6Al-7Nb alloy are surface hardened and the improvement of micro-hardness range from 365 HV_{0.05} to 425HV_{0.05}. Yin et al.,²⁹ examined the effects of LSP on microhardness of Ti-6Al-4V. The microhardness was improved from 390 HV_{0.5} to 470HV_{0.5}, due to two factors which separately are a severe plastic layer was generated and the grain refinement according to Hall-Petch formula.

If we keep the overlap constant, looking at the microhardness distribution according to laser energy we can see that the depth of the surface hardened layer and microhardness are proportional to the laser energy. For instance, at 33%, 7J laser-induced around 410

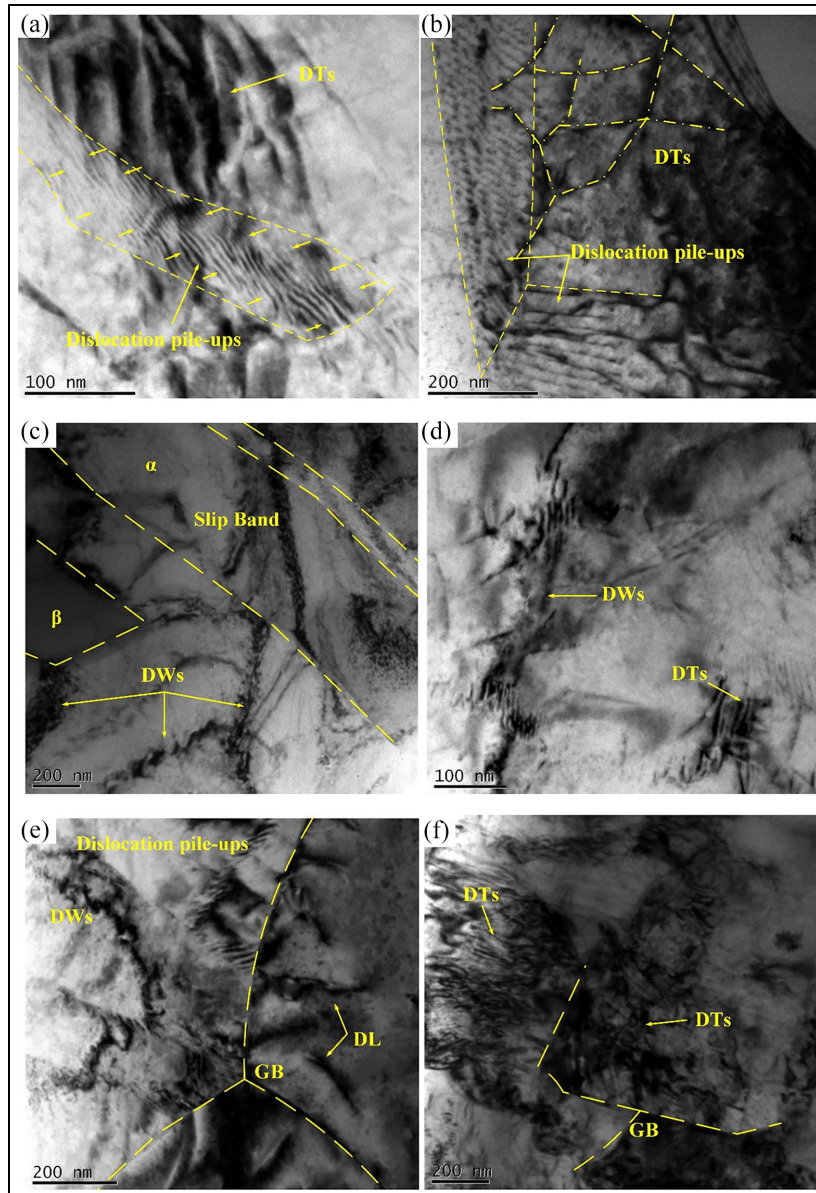


Figure 6. TEM image showing (a) -(b) dislocation pile-ups; (c)-(e) Slip band dislocation tangles; and (e)-(f) dislocations near the grain /sub-grain boundary.

$HV_{0.05}$ at the near-surface followed by 375 $HV_{0.05}$ (5 J) and 365 $HV_{0.05}$ (3 J). The microhardness decreases gradient along the depth direction, eventually, leading to a stable value as same as the untreated means the surface hardened effect are disappeared beyond this point. Ge et al.,³⁰ laser peened the magnesium with 6.5, 8.5 and 10.5 J laser energy. The plastic deformation layer depths at three different laser energies are 0.6, 0.7, and 0.8 mm, respectively. The surface hardened effect will reduce along the cross-section direction and the affected depth is called plastic deformation layer. A similar trend was also be found in 50% and 67% curves. Amongst these three overlaps, we can see that the gap in the 67% curves are much narrow which means the surface hardened effect is not so obviously improved by 7 J laser.

By keeping laser energy constant, it can be seen that microhardness and surface hardness depths are also proportional to overlap. For example, the microhardness of 3 J at the near-surface is 365 $HV_{0.05}$ (33%), 372 $HV_{0.05}$ (50%) and 377 $HV_{0.05}$ (67%). In 5 and 7 J, the microhardness at the near-surface was improved to 374 $HV_{0.05}$ (5 J, 33%), 389 $HV_{0.05}$ (5 J, 50%), 402 $HV_{0.05}$ (5 J, 67%) and 409 $HV_{0.05}$ (7 J, 33%), 416 $HV_{0.05}$ (7 J, 50%) 425 $HV_{0.05}$ (7 J, 67%).

Wear behaviour in simulated body fluid

Wear behaviour. Figure 10 shows the COF versus number fretting wear cycles of Ti-6Al-7Nb alloy subject to LSP parameter of 7 J group in SBF. All laser

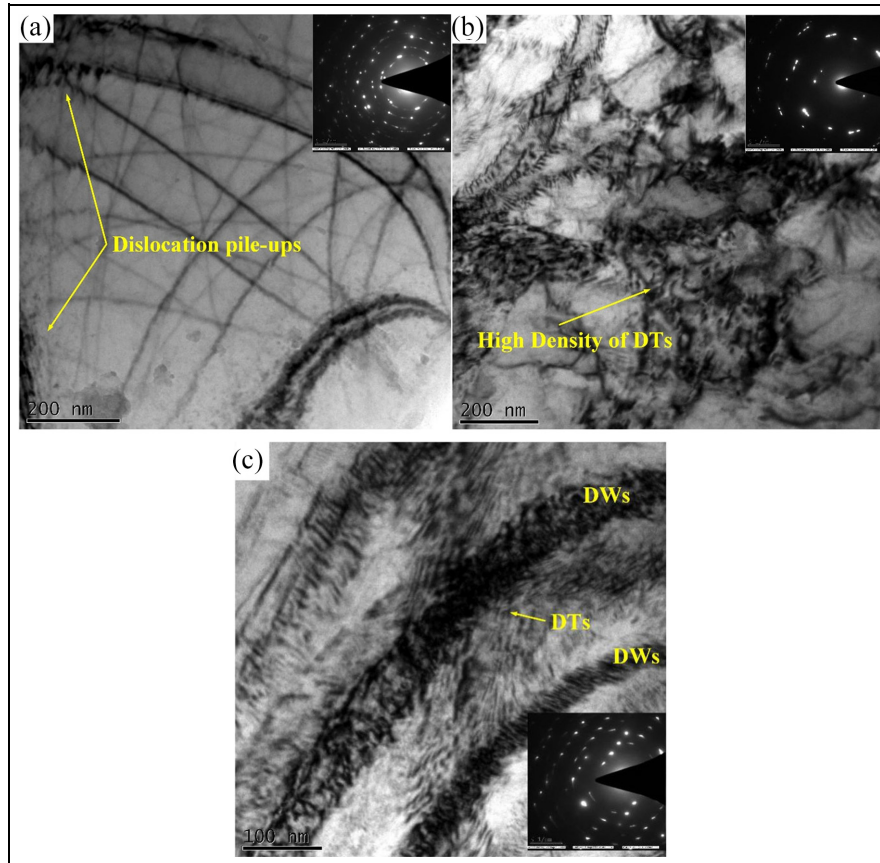


Figure 7. The TEM images showing the microstructure of laser shock peened Ti-6Al-7Nb at the top surface (a) and sub-surface (b and c) corresponding selected area electron diffraction separately.

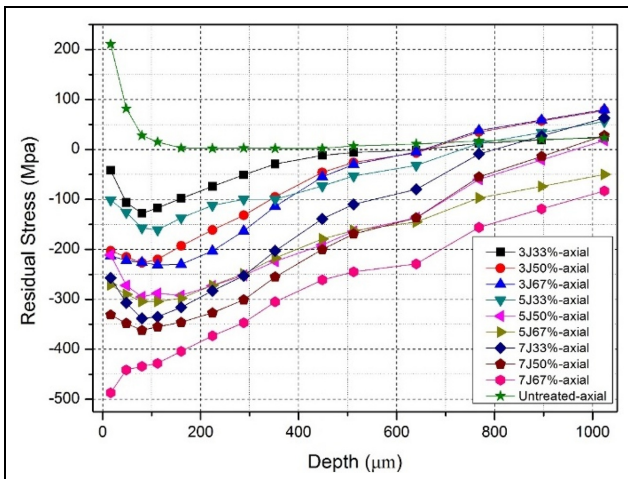


Figure 8. A plot showing the cross-sectional distributions of axial directional residual stress of Ti-6Al-7Nb before and after LSP.

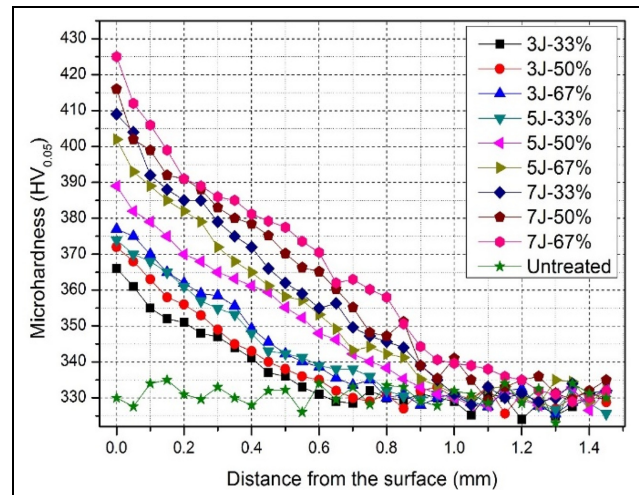


Figure 9. The microhardness map showing the through thickness microhardness distribution of Ti-6Al-7Nb alloy before and after multiple laser shock peening in surface and sub-surface.

shock peened curves are similar which are characterised by an initial run-in stage with a sharp increase, followed by a steady-state regime. As shown in Figure 10(b), it was found that in the run-in step, the untreated curve increases faster than that of laser shock peened curves. This can be attributed to the surface hardness induced by LSP. A low COF indicated an easy sliding

of two contacting bodies. However, with the increasing number cycles of wear tests, there is no obvious difference amongst the untreated and laser shock peened samples in 3 and 5 J groups when they gradually stabilised in the steady-state step. As present in the microhardness section, the surface hardened depth after 3

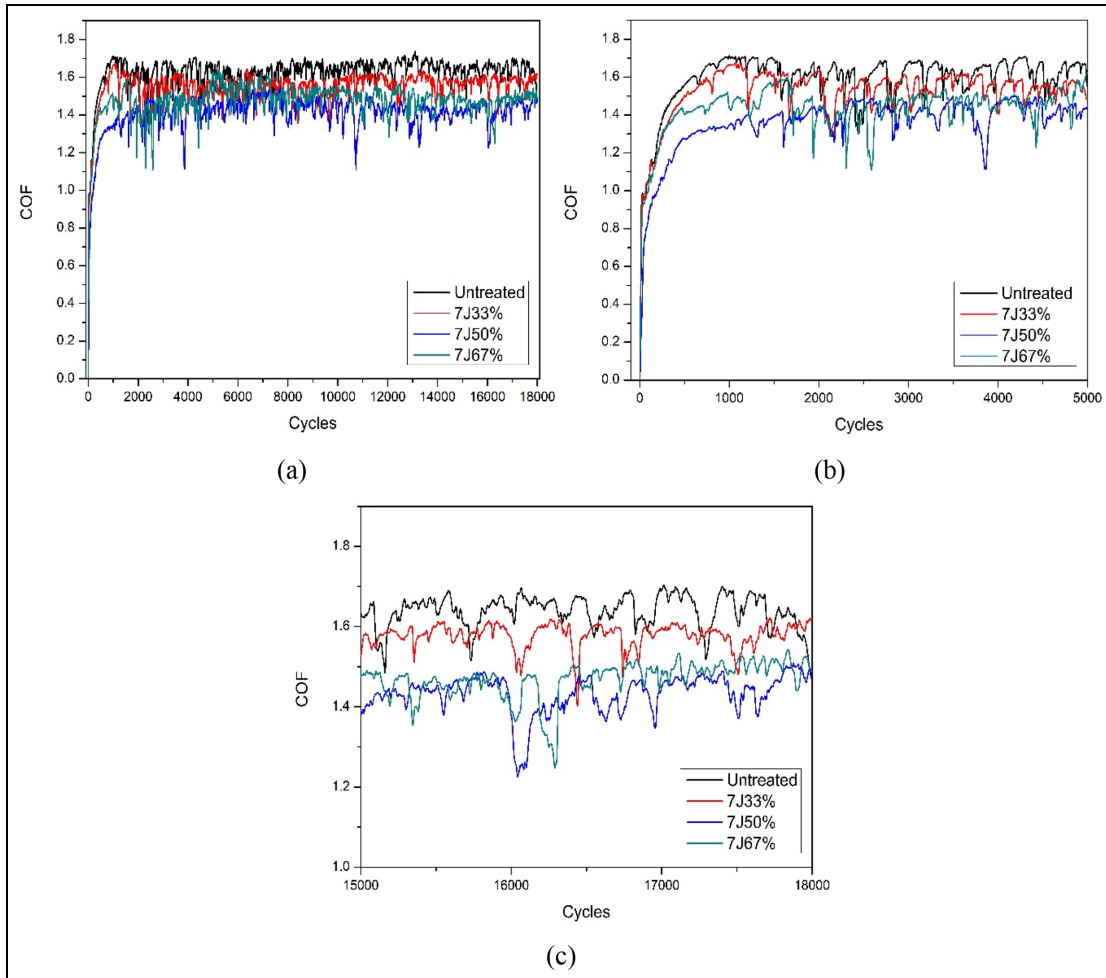


Figure 10. Comparative plot showing the friction co-efficient (COF) versus number of cycles for Ti-6Al-7Nb alloy before and after laser shock peening in 7J, 33%; 7J, 50%; 7J, 67% (a); the magnified run-in stage in (b); the magnified steady-state step shown in (c).

and 5J LSP is comparatively shorter than that of 7J. What is more, although surface hardness was induced by LSP, the surface roughness was also increased which was detrimental to the wear resistance. Once the cycles are more than certain values, the surface hardened layer of 3 and 7J samples have already worn out, whereas, the worn surface was the matrix and that was why COFs of the laser shock peened was very closed to that of the untreated.

When it comes to 7J groups (Figure 10), at the run-in stage (Figure 10(b)), COFs of untreated also increased higher than that of the laser shock peened samples. However, in the steady-state step, we can see that the average of COFs of laser shock peened samples are all lower than that of untreated. In addition, the gradient decreasing sequence can be observed that the sequence is 7J, 33% > 7J, 50% ≈ 7J, 67%.

COFs of 7J, 50% and 7J, 67% are comparatively close to each other. What is more, the wear volume loss of Ti-6Al-7Nb samples before and after LSP are calculated with maximum worn depth and presented in Figure 11. The wear volume loss of the untreated surface is $5.72 \times 10^{-3} \text{ mm}^3$. In comparison to the untreated

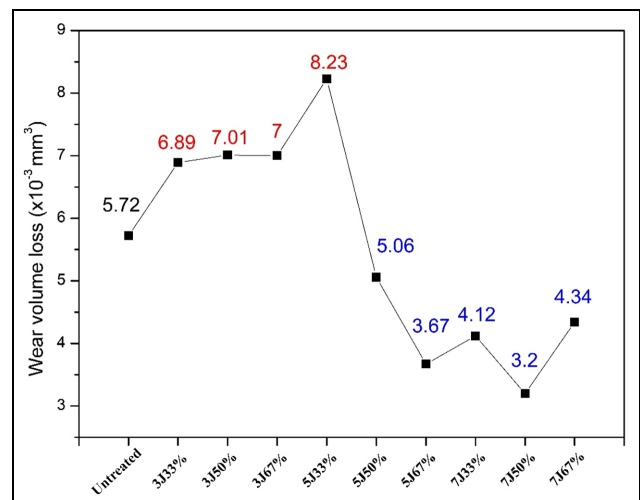


Figure 11. The plot showing wear volume loss of Ti-6Al-7Nb alloy before and after laser shock peening.

surface, 5J, 33% lost the maximum volume amongst all the laser shock peened samples with a value of $8.23 \times 10^{-3} \text{ mm}^3$, followed by 3J, 50%, (7.01×10^{-3}

mm³), then 3 J, 67% (7×10^{-3} mm³) and finally 3 J, 33% (6.89×10^{-3} mm³) that the wear volume loss are higher than that of the untreated. Once the laser energy and overlap are increased to 5 J, 50%, the wear resistance effect of LSP start to show. Marked by blue in the Figure 11 which values are lower than that of the untreated surface, 7 J, 50% experienced the minimum volume loss (3.2×10^{-3} mm³), onwards is 5 J, 67% (3.67×10^{-3} mm³), 7 J, 33% (4.12×10^{-3} mm³), 7 J, 67% (4.34×10^{-3} mm³) and 5 J, 50% (5.06×10^{-3} mm³). It is well-known that enhanced hardness and microstructural refinement are both induced after LSP surface treatment to ultimately, improve wear resistance, but the surface roughness is also increased which is detrimental to wear performance. Although, the surfaces are hardened and the average size of sub-grains are minimised, the wear volume loss is still higher after the LSP. This is because of the increase of surface roughness after LSP. In addition, the wear volume loss of sample 5 J, 33% is comparative close to the one of the untreated sample. Therefore, it can be considered as a neutralised result among roughness (negative to the wear resistance), surface hardness and microstructure refinement (positive to the wear resistance).

The worn surfaces. According to the worn surfaces, Ti-6Al-7Nb samples can be divided into 3 categories which are: (1) the untreated and treated at 5 J, 50%; (2) 3 J, 33%, 3 J, 50%, 3 J, 67% and 5 J, 33%; (3) 5 J, 67%, 7 J, 33%, 7 J, 50% and 7 J, 67%. Therefore, Figure 12 shows the typical appearance of fretted scars on Ti-6Al-7Nb before and after LSP (including untreated, 5 J, 33% and 7 J, 67%). This is consistent with the wear volume loss. As shown in Figure 12(a), the ploughing wear mechanism dominated in the wear process of the untreated and 5 J, 50%. In the high magnification images, the micro-ploughing and spalling features on the abraded surfaces can be seen. With respect to the samples 3 J, 33%, 3 J, 50%, 3 J, 67% and 5 J, 33%, as exhibited by Figure 12(b), the worn surfaces exhibited much more severe wear among the others. Extensive debris, grooves, material adhesions and delamination were found after the adhesive and abrasive wear along the sliding wear direction. Although the hardened surface layer in laser shock peened samples benefited the wear resistance, the asperities on the surface induced by LSP facilitated the removal of the top material off the surface. Compared to that, as shown in Figure 12(c), 7 J, 50% exhibits less wear in the SBF as the surface hardening at least is increased to 400 HV_{0.05}. This enable them to get better performance in wear. From the worn SEM images, adhesion and abrasive wear still co-existed on the worn surfaces as the adhesion material, spalling, and delamination was found. However, the delamination area ratio is proportional to the wear volume loss. Especially in 7 J, 50%, from the SEM image, the wear scar consists of most delamination and less adhesion material. Therefore, it was seen that the delamination wear is the main wear mechanism.

In general, the diameter of the wear scars are proportional to the wear scar depth as shown in Figure 13. However, some samples such as 3 J, 67% and 5 J, 33% are not consistent with that trend. This may be due to the FBS environment. The wear is a process that the removal of the passive oxide layer exposing the metallic surfaces, thereby, undergoing anodic dissolution. As such, the wear scar acts as a cathode. The body simulated solution aggravates the anodic dissolution and material removal during the wear process. What is more, in the present study, the wear results is a neutralisation result amongst surface roughness, surface hardness and the microstructural refinement. In terms of wear scar depth, limited surface hardening with low surface roughness may not be worse than higher surface hardening with higher surface roughness. That is why the two set of parameters in the middle exhibit the maximum wear scar depth.

Wettability

The advancing contact angle of Ti-6Al-7Nb titanium before and after LSP with distilled water is presented in Figure 14. As a base line, the contact angle of untreated samples with distilled water of 53.96°. Comparing this, all laser shock peened contact angles are higher than the untreated which was also concluded in the work of Prabhakaran et al.³¹ and Caralapatti and Narayanswamy.³² The highest water contact angle is 79.94°, which was 3 J, 33%. Meanwhile, the lowest for water was 64.09°, at 7 J, 67%. What is more, observing the figure form longitudinal direction, contact angle values rise with the increase of laser energy at the same overlap. However, in the transverse way, the contact angles decreased with the increase of overlap at the same laser energy level.

Cell morphology and viability

Figure 15 presents the fluorescence images of the attached cells on the titanium surfaces prior to and after LSP after 72 h. It was seen that the morphology of cells was well distributed on both surfaces prior to and after LSP. In the Figure 15(b) to (d) (3 J group from 33% to 67% overlap), the cell numbers are increased with the respective laser overlap. However, compare to the untreated, the cell numbers are quite lower after 3 J, laser energy processing. In 5 J groups (Figure 15(e)–(g)), the cell numbers are not increased with overlap as cells on the 50% (Figure 15(f)) and 67% (Figure 15(g)) are comparatively lower than that of 5 J, 33% (Figure 15(e)) overlap. In comparison to the untreated surfaces, the numbers in 5 J, 33% and 5 J, 67% are higher than that of the untreated surface. In terms of 7 J groups (7 J, 33%, 7 J, 50% and 7 J, 67%), only the cell numbers in 7 J, 33% (Figure 15(h)) is lower than that of the untreated surface and the lowest among the three variables. 7 J, 50% (Figure 15(i)) and 7 J, 67% (Figure 15(j)) are comparatively close to each other.

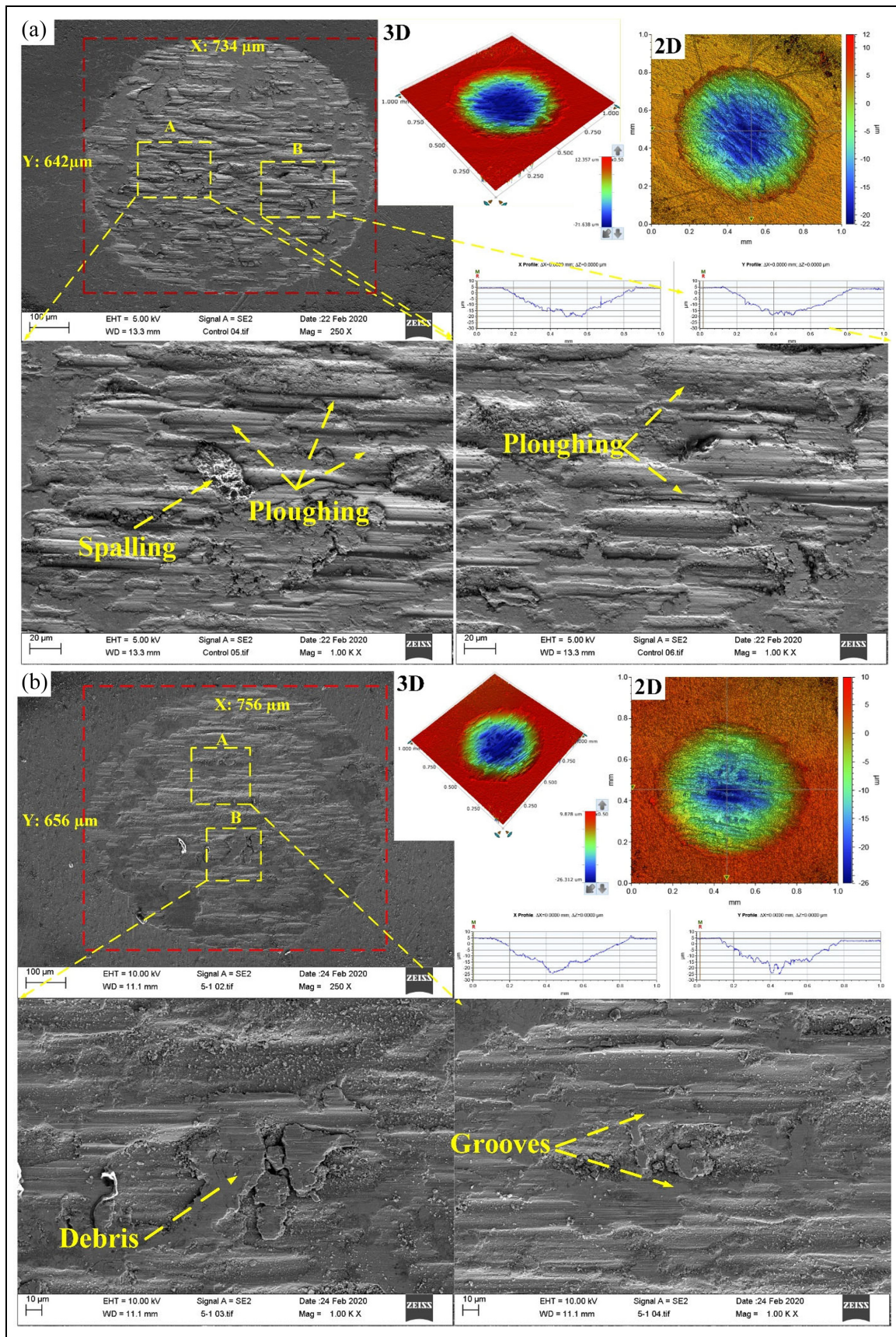


Figure 12. (Continued)

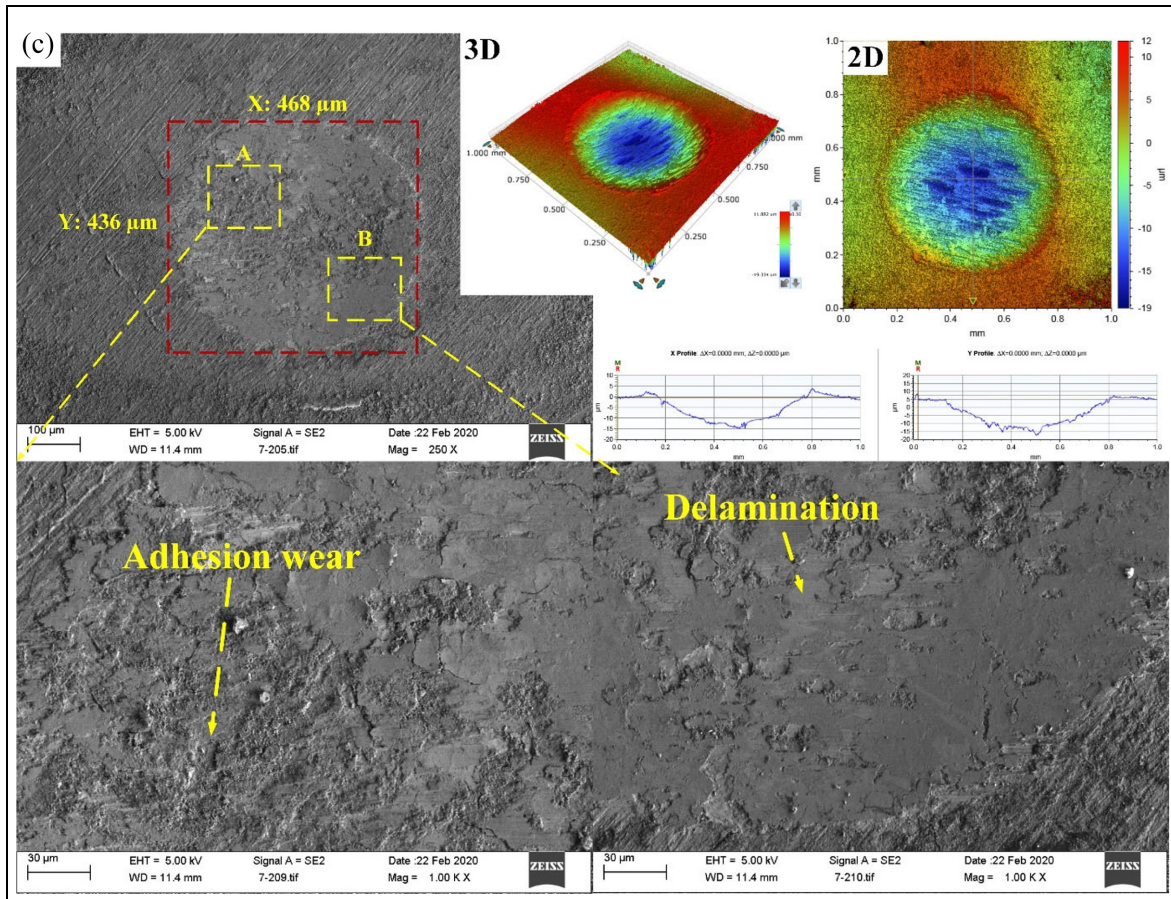


Figure 12. SEM and 3-D profiling maps showing the wear scar of Ti-6Al-7Nb alloy prior to and after LSP: (a) the untreated surface, (b) at 5J, 33% and (c) 7J, 50%.

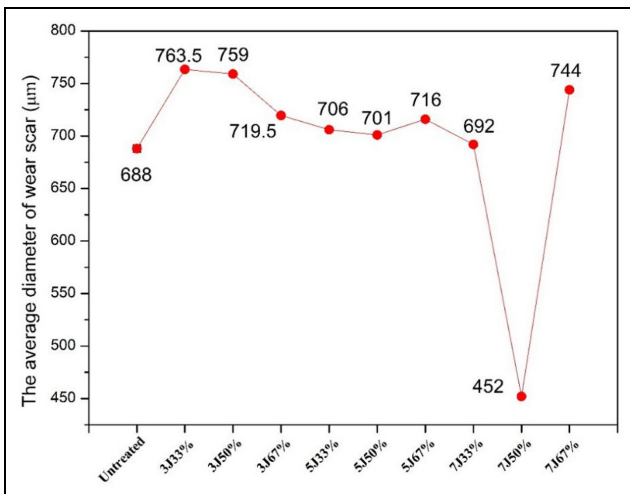


Figure 13. The plot showing the average diameter of wear scars for Ti-6Al-7Nb alloy before and after laser shock peening.

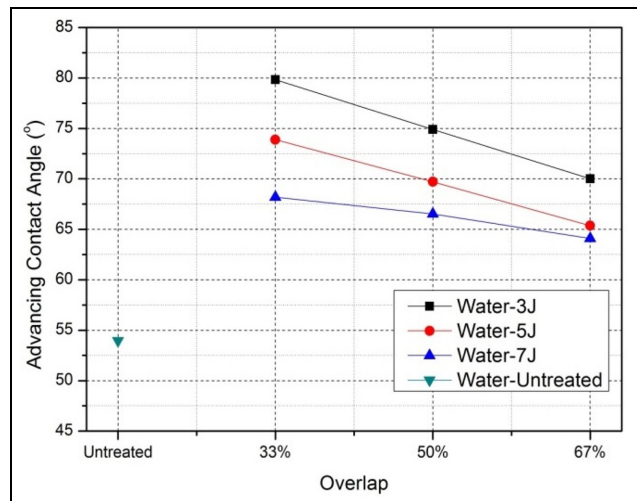


Figure 14. Advancing contact angle on both untreated and laser shock peened specimens for distilled water.

Figure 16 presents the cell viability of MG-63 cells after 24 and 72 h on the as-control and the laser shock peened surface with MTT assay. Overall, it was observed that the cells can attach onto both surfaces of

untreated and the laser shock peened surfaces. This meant that LSP was not cytotoxic to Ti-6Al-7Nb alloys. Then, in the data for 24h group, except 5J, 33% and 7J, 67%; the optical density value of the rest

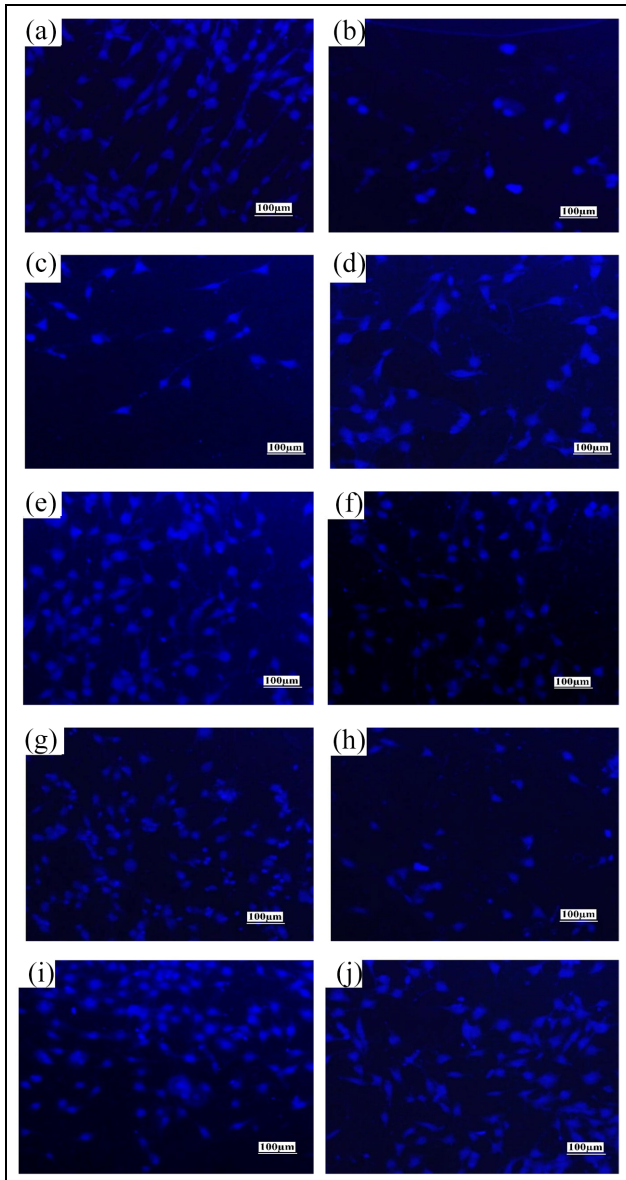


Figure 15. Fluorescence image showing cell morphology prior to and after Ti-6Al-7Nb alloy incubated for 72 h: (a) Untreated, (b) 3J, 33% overlapping, (c) 3J, 50%, (d) 3J, 67%, (e) 5J, 33%, (f) 5J, 50%, (g) 5J, 67%, (h) 7J, 33%, (i) 7J, 50% and (j) 7J, 67%.

of the laser shock peened are all lower than untreated. This means the cell viability in the above samples were not higher than that of the untreated. There it indicates that laser overlap is correlated with the cell viability after laser peening surface treatment with these particular parameters.

After 72 h, it was observed that all optical density values of the laser shock peened surfaces were equal to or higher than that of untreated. 5 J, 50% reached the highest cell growth with a mean value of 0.82, followed by 5 J, 33% (0.79), 3 J, 67% (0.73) and 7 J, 50% (0.712).

Discussion

The fluorescence images suggest that not all LSP parameters are beneficial to the osseointegration of implant

materials, despite having a high level of compressive residual stress. It was observed that cell numbers after some LSP were much lower than that of the untreated in the confocal images. These LSP parameters were: 3 J, 33%, 3 J, 50%, 3 J, 67%, 5 J, 50%, and 7 J 33%. Furthermore, in the 1 day MTT result, cell viability of 3 J groups, 5 J, 50%, 7 J, 33% and 7 J, 50% are comparatively close to or lower than that of the untreated. This was postulated due to the differences amongst the surface morphologies after LSP. From another point of view, LSP surface treatment can work as a filter function that LSP selects high viability cell and eliminates the unhealthy cells and in turn, could render greater benefits. This meant in the early stages, certain LSP parameters are detrimental to the cell number, and somehow, the cell on the laser shock peened surfaces will decrease. These results are also in agreement with the work of Bagherifard et al.,³³ who seeded osteoblast cells on shot peened and untreated surfaces for 1, 3 and 7 days. It was found that after 1 and 3 days, the viability of the cells of shot peened were lower than that of the untreated. Even after 7 days culture, there were still no significant improvements after shot peening on the surfaces. However, in our study, compared to 24 h result, the cell viabilities of all laser shock peened surfaces were significantly increased after 72 h, while the untreated surfaces of Ti-6Al-7Nb, were slightly decreased. This might be due to the rough surface that must be beneficial to the bone-implant interface osseointegration. It is the micro features such as dimples, grooves and nano features (reliefs) induced by LSP that improved the cell viability on the treated surfaces. Moreover, the increased value was found to be comparatively large in 3 J group, and sample treated at 5 J, 50%.

Overall, amongst nine LSP parameters, three of them (5 J, 33%, 5 J, 67% and 7 J, 6%), exhibited consistent performance in both 24 and 72 h experiments. Compared to the untreated; the increase of 5 J, 67% and 7 J, 67%, are not obvious. In addition, after considering the performance in 24 h experiments, although, 5 J, 50%, was the highest (0.82) in 72 h experiment, 5 J, 33% was the optimal LSP parameters for cell viability as it rendered high cell viability from evaluating all the experiments.

It has been reported in the literatures that the biocompatibility of the implant was affected by surface finishing, and the corresponding surface wettability. Surface topographies were characterised by parameters such as root mean squared, maximum valley depth, maximum peak height and skewness etc. With that said, the parameters of 3-D mean average roughness S_a were the most used to present implant surface finishing. However, such parameters are not suitable to stand for the periodic surface structures after surface modification as different surface morphologies may have the same surface roughness with totally different wetting properties. Therefore, in this study, considering the relationship between the cell viability and the overlap is

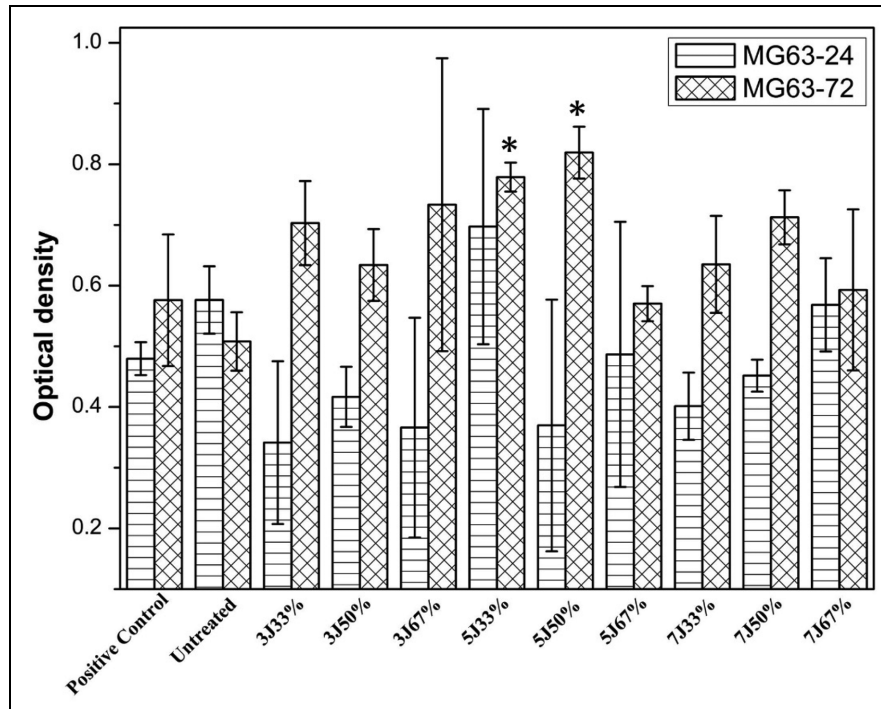


Figure 16. shows the absorbance of MG-63 cells on the surfaces of positive control, untreated and the laser shock peened for 24 and 72 h (Data = mean \pm St. Dev; $N = 3$, * $p < 0.05$ compared to the positive control at the same time point).

not appropriate as the surface morphologies induced by overlap vary from each other at the same laser energy. Up on keeping the overlap consistent and laser energy variable was because the surface morphologies are nearly with varying in the depth of the valley and the height of the peak. It is more reasonable to analyse the relationship by keeping the overlap consistent. Figure 17 showed the scatter distribution of the contact angle (water) versus the optic density. It can be seen that the highest cell viability exhibits in the range between contact angles of 70° – 75° . In 33%, 50% and 67% laser overlapping groups, 5 J, 33%, 5 J, 50% and 3 J, 67%, present the highest cell viability in the range. If the contact angle is lower than 70° or higher than 75° , the cell viability will comparatively be lower than that in this range. The fitted third-degree polynomial equation indicated that the optimal contact angle should be located at 71.56° . Tamada and Ikada,³⁴ found that the optimal water contact angle for cell adhesion was approximately 70° , which was in good agreement from the results of our research herein. From the above discussion, surface wetting properties is the directly influential factor while the surface roughness was also determining the cell viability via surface wetting properties. This is because, surface roughness is also an important factor that determines the surface wettability.

Combining with the mechanical, interfacial results, properties such as biocompatibility, mechanics, and wettability cannot all be benefited by only one simple LSP parameter. For example, with respect to residual

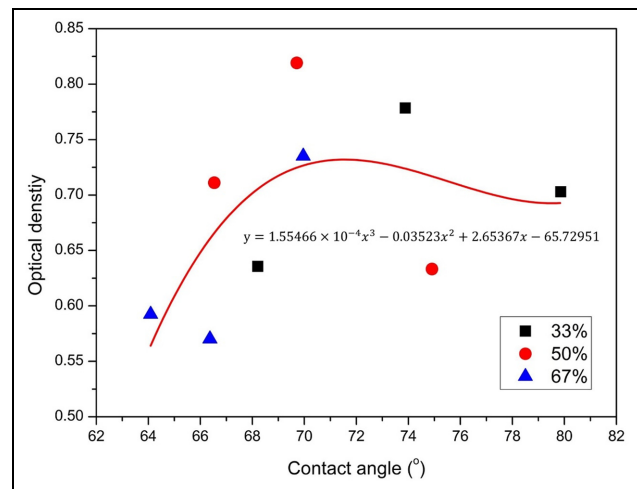


Figure 17. Plot of contact angle versus optical density with the fitting equation.

stress and microhardness, 7 J, 67% are optimal LSP parameters leading to maximum compressive residual stress and surface hardening. However, such benefits may not necessarily produce the best surface morphology that creates a beneficial biological response. The morphology may also affect the wettability by increasing the contact angle. Therefore, the evaluations of the performance post different LSP conditions need to be considered comprehensively, with a particular requirement and or a specification. It has to be compromised between mechanical and biological properties.

Table 4. The pros and cons of laser shock peening on cell viability and wear resistance.

	Wear resistance	Cell viability
3J, 33%	×	√√
3J, 50%	×	√
3J, 67%	×	√√
5J, 33%	××	√√
5J, 50%	-	√√
5J, 67%	√√	√
7J, 33%	√√	√
7J, 50%	√√√	√√
7J, 67%	√√	-

×: Worse than the untreated; -: Comparatively closed to the untreated; √: Better than the untreated.

Regarding the LSP parameters of 3 J, although, the cell viability after 72 h was higher than that of 7 J treated surfaces, the wear resistance was inadequate after LSP. This is not acceptable for the medical industry applications as wear debris may be worn out inside the human body, leading to early failure of the implant. Thus, low laser energy is not applicable for improving the wear resistance.

In the 5 J LSP group, regarding cell viability performance, 5 J, 33% and 5 J, 50% were comparatively better than 5 J, 67%. With that said, the wear loss volumes are higher due to the lower surface hardening. Especially, the wear volume loss of 5 J, 33% was the highest amongst all LSP samples. In other words, compared to the untreated, 5 J, 67% improved the wear resistance, but did not enhance the cell viability. The surfaces treated with 5 J, 50% compromised of wear volume loss and rendered cell viability. As for 72 h culture, the cell viability is the highest amongst samples post all LSP parameters with the comparative low wear loss volume. For further improvement, multiple LSP impacts can be applied to the 5 J, 50% for the deeper surface hardening layer, thereby, enhancing the wear resistance.

As mentioned above, 7 J samples received the deepest surface hardening and exhibited the best performance in wear resistance. However, the improvements of the cell viability are comparatively lower than that of other LSP parameters. This is due to the decrease of contact angle leading to contact angle value lower than 70°. The pros and cons of LSP on cell viability and wear resistance are summarised in Table 4. It can be seen that compromising the results of the cell viability and wear resistance, 7 J, 50% was the optimal LSP parameter for improving the comprehensive properties of Ti-6Al-7Nb alloy.

Conclusions

This paper focuses on laser shock peening, a medical-grade Ti-6Al-7Nb alloy with a range of laser energies (3, 5 and 7 J) and overlaps (33%, 50% and 67%) with

a spot-size of 3 mm, 20 ns pulse duration and a frequency of 5 Hz. The evaluation was carried out from microstructural, mechanical, interfacial and biological aspects. The corresponding conclusions were drawn as follows:

- By LSP, the average sub grain size can be refined to 36.8% at maximum. The evaluation of phase transformation revealed that there was no new phase formed after LSP. The peak was broadened with increasing the energy, whilst keeping the overlap constant. Dislocation tangles, dislocation walls, dislocation cells and dislocation pile-ups were observed using TEM. According to Hall-Petch theory, these deformation features benefit the mechanical properties of Ti-6Al-7Nb alloy after performing laser shock peening.
- The surface was hardened after LSP. Laser energy and overlap were proportional to microhardness at the near-surface. LSP parameters of 5 J, 67%, 7 J, 33%, 7 J, 50% and 7 J, 67% all improved the wear resistance in SBF, while parameters of 3 J, 33%, 3 J, 50%, 3 J, 67% and 5 J, 33% could aggravate the implant failure due to wear. LSP induced surface roughness is detrimental to the wear resistance of Ti-6Al-7Nb alloy, if the surface hardening effect is not enough.
- From fluoresce images after 72 h culture experiment, it was seen that LSP surface treatment was not toxic to MG63 cell adhesion. There is not a dramatic increase in the cell numbers on both surfaces before and after LSP. By contrast, the cell numbers of non-optimal LSP parameters are even quite lower than that of untreated surfaces. The MTT assay results showed that, after 72 h the cell viability of laser shock peened samples are all higher than that of untreated. The cell viability is directly related to the surface wetting properties as more contact angle is close to 71.5°, the higher the cell viability it presents.
- Considering with both mechanical and biological performance, 7 J, 50% is the optimal LSP processing parameters for improving the implant properties.

This work has shown that laser shock peening has a potential to be deployed to improve the implant osseointegration, as it not only improves the mechanical properties, but also, the cell viability. However, such cell viability, for example the culture days are not enough to “characterize the biocompatibility of laser shock peened titanium samples. Further work is underway to verify/confirm this with additional biological experiments, namely: mesenchymal stem cell proliferation, adhesion, and differentiation.

Acknowledgements

We would like to thank Prof. S. Kalainathan and Prof. Geetha Manivasagam from Vellore Institute of

Technology for the access to X-Ray diffraction and corresponding biological experiment and equipment.

Author contributions

Xiaojun Shen: Investigation, Methodology and Writing the original draft. Pratik Shukla: Methodology, Funding acquisition, Review and Editing and helping the preparation of a draft and corresponding author. Sunita Nayak: Investigation, Review and Editing. Vasanth Gopal: Investigation, Methodology. S Prabhakaran: Investigation, Methodology. Amy Sarah Benjamin: Investigation. S Kalainathan: Funding acquisition.


Declaration of conflicting interests

The author(s) declared no potential conflicts of interest with respect to the research, authorship, and/or publication of this article.

Funding

The author(s) disclosed receipt of the following financial support for the research, authorship, and/or publication of this article: The corresponding author of this paper would like to thank the Engineering Physical Sciences Research Council (EPSRC) funded laser loan pool scheme and also the Science & Technology Facilities Council (STFC) for granting a state-of-the-art system for Laser Shock Peening applications (Grant no: EP/G03088X/1 (13250017 - NSL4)), which was manufactured by Litron Lasers Ltd.

ORCID iD

Pratik Shukla  <https://orcid.org/0000-0002-3986-2316>

References

- Hudecki A, Kiryczyński G and Łos MJ. Chapter 7 - biomaterials, definition, overview. In: Łos MJ, Hudecki A and Wiecheć E (eds) *Stem cells and biomaterials for regenerative medicine*. Cambridge, MA: Academic Press, 2019, pp.85–98.
- Chen S, Guo Y, Liu R, et al. Tuning surface properties of bone biomaterials to manipulate osteoblastic cell adhesion and the signaling pathways for the enhancement of early osseointegration. *Colloids Surf B Biointerfaces* 2018; 164: 58–69.
- Flamant Q, García Marro F, Roa Rovira JJ, et al. Hydrofluoric acid etching of dental zirconia. Part 1: etching mechanism and surface characterization. *J Eur Ceram Soc* 2016; 36: 121–134.
- Günay-Bulutsuz A, BerrakÖ, Yeprem HA, et al. Biological responses of ultrafine grained pure titanium and their sand blasted surfaces. *Mater Sci Eng C* 2018; 91: 382–388.
- Granato R, Bonfante EA, Castellano A, et al. Osteointegrative and microgeometric comparison between microblasted and alumina blasting/acid etching on grade II and V titanium alloys (Ti-6Al-4V). *J Mech Behav Biomed Mater* 2019; 97: 288–295.
- Mukherjee S, Dhara S and Saha P. Enhancing the biocompatibility of Ti6Al4V implants by laser surface microtexturing: an in vitro study. *Int J Adv Manuf Technol* 2015; 76: 5–15.
- Raimbault O, Benayoun S, Anselme K, et al. The effects of femtosecond laser-textured Ti-6Al-4V on wettability and cell response. *Mater Sci Eng C* 2016; 69: 311–320.
- Batal A, Sammons R and Dimov S. Response of saos-2 osteoblast-like cells to laser surface texturing, sandblasting and hydroxyapatite coating on CoCrMo alloy surfaces. *Mater Sci Eng C* 2019; 98: 1005–1013.
- Xiong Y-Z, Gao R-N, Zhang H, et al. Rationally designed functionally graded porous Ti6Al4V scaffolds with high strength and toughness built via selective laser melting for load-bearing orthopedic applications. *J Mech Behav Biomed Mater* 2020; 104: 103673.
- Shen X, Shukla P, Nath S, et al. Improvement in mechanical properties of titanium alloy (Ti-6Al-7Nb) subject to multiple laser shock peening. *Surf Coat Technol* 2017; 327: 101–109.
- Clauer AH. Laser shock peening, the path to production. *Metals* 2019; 9: 626.
- Gujba AK and Medraj M. Laser peening process and its impact on materials properties in comparison with shot peening and ultrasonic impact peening. *Materials* 2014; 7: 7925–7974.
- Attia MH. Effect of laser surface treatment and work hardening on the fretting wear resistance of Zr-2.5Nb alloy at high temperature. In: Hassan MF and Megahed SM (eds) *Current advances in mechanical design and production VII*. Oxford: Pergamon, 2000, pp.521–529.
- Basseville S and Cailletaud G. An evaluation of the competition between wear and crack initiation in fretting conditions for Ti-6Al-4V alloy. *Wear* 2015; 328–329: 443–455.
- Royhman D, Patel M, Runa MJ, et al. Fretting-corrosion in hip implant modular junctions: new experimental setup and initial outcome. *Tribol Int* 2015; 91: 235–245.
- Zhou J, Sun Y, Huang S, et al. Effect of laser peening on friction and wear behavior of medical Ti6Al4V alloy. *Opt Laser Technol* 2019; 109: 263–269.
- Zhang R, Zhou X, Gao H, et al. The effects of laser shock peening on the mechanical properties and biomedical behavior of AZ31B magnesium alloy. *Surf Coat Technol* 2018; 339: 48–56.
- Luo KY, Wang CY, Cui CY, et al. Effects of coverage layer on the electrochemical corrosion behaviour of Mg-Al-Mn alloy subjected to massive laser shock peening treatment. *J Alloys Comp* 2019; 782: 1058–1075.
- Shukla PP and Lawrence J. Identification of optical parameters for determination of radiance. *J Opt* 2015; 44: 12–19.
- Acharya S, Panicker AG, Gopal V, et al. Surface mechanical attrition treatment of low modulus Ti-Nb-Ta-O alloy for orthopedic applications. *Mater Sci Eng C* 2020; 110: 110729.
- Grant PV, Lord JD and Whitehead PS. *Measurement good practice guide no. 53*. Teddington: National Physical Laboratory, 2002.
- ASTM. *Standard test method for determining residual stresses by the hole-drilling strain-gage method*. American Society for Testing and Materials, West Conshohocken 2008, pp.837–895.
- Kang JM, Wang YH, Chen XM, et al. Grain refinement and mechanical properties of Fe-30Mn-0.11C steel. *Results Phys* 2019; 13: 102247.

24. Wang C, Shen XJ, An ZB, et al. Effects of laser shock processing on microstructure and mechanical properties of K403 nickel-alloy. *Mater Des* 2016; 89: 582–588.
25. Yang Y, Zhou K and Li G. Surface gradient microstructural characteristics and evolution mechanism of 2195 aluminum lithium alloy induced by laser shock peening. *Opt Laser Technol* 2019; 109: 1–7.
26. Yang Y, Lian X, Zhou K, et al. Effects of laser shock peening on microstructures and properties of 2195 Al-Li alloy. *J Alloys Comp* 2019; 781: 330–336.
27. Zhou L, He W, Luo S, et al. Laser shock peening induced surface nanocrystallization and martensite transformation in austenitic stainless steel. *J Alloys Comp* 2016; 655: 66–70.
28. Shen X, Shukla P, Subramaniyan AK, et al. Residual stresses induced by laser shock peening in orthopaedic Ti-6Al-7Nb alloy. *Opt Laser Technol* 2020; 131: 106446.
29. Yin M-G, Cai Z-B, Li ZY, et al. Improving impact wear resistance of Ti-6Al-4V alloy treated by laser shock peening. *Trans Nonferrous Met Soc China* 2019; 29: 1439–1448.
30. Ge MZ, Xiang J-Y, Tang Y, et al. Wear behavior of Mg-3Al-1Zn alloy subjected to laser shock peening. *Surf Coat Technol* 2018; 337: 501–509.
31. Prabhakaran S, Kulkarni A, Vasanth G, et al. Laser shock peening without coating induced residual stress distribution, wettability characteristics and enhanced pitting corrosion resistance of austenitic stainless steel. *Appl Surf Sci* 2018; 428: 17–30.
32. Caralapatti VK and Narayanswamy S. Analyzing the effect of high repetition laser shock peening on dynamic corrosion rate of magnesium. *Opt Laser Technol* 2017; 93: 165–174.
33. Bagherifard S, Hickey DJ, Fintová S, et al. Effects of nanofeatures induced by severe shot peening (SSP) on mechanical, corrosion and cytocompatibility properties of magnesium alloy AZ31. *Acta Biomater* 2018; 66: 93–108.
34. Tamada Y and Ikada Y. Cell adhesion to plasma-treated polymer surfaces. *Polymer* 1993; 34: 2208–2212.